JOURNAL OF SYNCHROTRON RADIATION
ISSN 1600-5775

One-dimensional parallax-free position-sensitive detector for diffraction measurements based on a home-made thin THGEM

Shi Chen,[a] Hongbang Liu,[b] Qian Liu,[a]* Yangheng Zheng,[a] Binglong Wang,[a] Wenqian Huang,[a] Yang Dong,[c] Yu Rong,[c] Xinda Jiao,[c] Yu Guan,[c] Jing Wang,[c] Min Li,[c] Jizhou Liu[d] and Mengmeng Zhang[d]

[a]University of Chinese Academy of Sciences, Beijing 100049, People's Republic of China, [b]Guangxi University, Nanning 530004, People's Republic of China, [c]Second Academy of China Aerospace Science and Industry Corporation, Beijing 100048, People's Republic of China, and [d]China Academy of Space Technology, Beijing 100048, People's Republic of China. *Correspondence e-mail: liuqian@ucas.ac.cn

Received 14 December 2017
Accepted 28 July 2018

Edited by S. Svensson, Uppsala University, Sweden

Keywords: micropattern gaseous detectors; thinner-THGEM; X-ray diffraction; BSRF.

A large parallax-free gas diffraction meter based on a thinner-THGEM (thick gaseous electron multiplier) has been developed at the Beijing Synchrotron Radiation Facility (BSRF). A thinner-THGEM of thickness 200 µm is adopted, which can be shaped into a curve to eliminate parallax-error effects. The detector is designed to have a 48° open angle positioned 20 cm from the powder samples. A front-end electronics board with 128 channels direct-current mode was adapted for the 8 keV BSRF beamline with 0.2 ns/100 ns stable duty cycle. Two powder samples, TiO_2 and SnO_2, were tested separately. The measured spectra with an angular resolution of $0.148 \pm 0.081^\circ$ are consistent with the data from the powder diffraction file. Combining the gas gain of the thinner-THGEM with the electronic circuit dynamic range, a very broad dynamic range of about 10^7 could be obtained.

1. Introduction

Synchrotron radiation offers an important tool for studying the structures of complex biological molecules, condensed materials and many others from different scientific domains. X-ray diffraction meters are devices commonly used for such studies. To study a diffraction spectrum, an adequate detector that can provide the necessary spatial resolution as well as dynamic range is needed, for example two-circle diffractometers (Cernik *et al.*, 1990; Collins *et al.*, 1992). At the Beijing Synchrotron Radiation Facility (BSRF) station, a five-circle diffractometer is used with a centimetre-size scintillator and one-channel photomultiplier tube signal output. The granularity of the scintillator defines the spatial resolution, and it is very time-consuming to reconstruct a single spectrum since the scintiallator has to be moved over the whole diffraction space. A large-sensitive-area detector can reduce the reconstruction time dramatically. For example, the Mar345 luminescence plate offers a relatively fast way to read out a circular sensitive area of diameter 345 mm in 150 s (Roessle *et al.*, 2007). Gas detectors such as the VANTEC-2000 provide a readout time of less than 0.2 s for a 140 mm × 140 mm area Moreover, a gas detector can be operated in ionization mode or avalanche mode, providing a much broader dynamic range. However, parallax errors induced from the gas detector have to be considered and calibrated. In this paper, we will introduce a one-dimensional parallax-free diffraction meter based on a thick gaseous electron multiplier (THGEM).

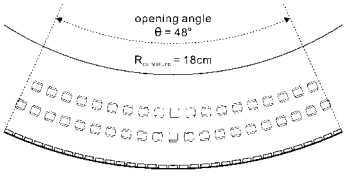

THGEMs are one of the novel micro-pattern gaseous detectors (MPGDs), devised in 2004 by Amos Breskin and co-workers (Chechik *et al.*, 2004). THGEMs are manufactured *via* standard printing circuit board (PCB) techniques and global etching processes. Their advantages include robustness, good spatial resolution (sub-millimetre), a high counting rate of 10^6 mm^{-1} s^{-1}, large volumes and low cost, making THGEMs a good choice for X-ray imaging experiments (Breskin *et al.*, 2009).

For X-ray diffraction measurements specifically, a flat-type gaseous detector will introduce a parallax error, which is caused by the uncertainty of the ionized depth when the electric field is not parallel to the direction of X-ray incidence (Duarte Pinto *et al.*, 2009). The parallax error at a particular diffraction peak resulting from this can be calculated using the formula $d\tan\theta/r$, where d is the depth of the drift region and θ is the diffraction angle. In principle, a curved shape can limit this effect. Here we propose a one-dimensional diffraction meter based on a thinner-THGEM. With a thickness of 200 µm, a thinner-THGEM can be easily curved and offers the possibility of maintaining a consistent X-ray incidence along the radial direction with the electron field line.

A thinner-THGEM detector was installed at the BSRF 1W1A diffuse X-ray scattering station and investigated using 8 keV X-rays. BSRF, a part of the Beijing Electron Positron Collider (BEPC) project, provides a free research platform for a large number of fundamental and applied research projects in the field of synchrotron radiation. BEPC commissioning has two modes, one being specific to collision physics and the other dedicated to BSRF usage in parasitic mode. In order to increase the time to be used for more stations with more working time, another mode, *i.e.* the compatible mode, can be used at certain BSRF stations with colliding commissioning simultaneously, but with slightly poorer beam parameters. The thinner-THGEM detector was tested during the compatible mode, with a beam size of 0.07 cm × 0.04 cm.

2. Thinner-THGEM

Thinner-THGEMs (Liu *et al.*, 2011) are obtained *via* standard PCB mechanical drilling and chemical etching processes. The thinner-THGEMs are 200 µm-thick FR-4 or G-10 boards with a thin copper layer of 18 µm on each side. A high density of holes of diameter 200 µm and pitch 500 µm are drilled. Small rims of less than 10 µm are etched around each hole to give a large and stable gain (Zhang *et al.*, 2012; Alexeev *et al.*, 2010). These thinner-THGEMs are thinner than regular THGEMs (usually 1 mm or thicker) and are flexible, thus making them easier to use for curved parallax-free detectors.

The structure of a one-dimensional thinner-THGEM is shown in Fig. 1. A thinner-THGEM film was positioned between two parallel electrodes. The upper electrode (cathode) is made of aluminium foil with a thickness of 20 µm. The lower electrode (anode) is a patterned PCB board with a thickness of 200 µm and readout pads with parallel strips of 400 µm width and 100 µm gap printed on the top of the PCB plate. The thicknesses of the drift and induction regions are adjusted to 2 cm and 0.2 cm, respectively.

A suitable electrical potential is applied to each foil. Working gas in the drift region is ionized by incident photons. The generated photoelectrons drift due to the electric field $E_{\rm drift}$, and are avalanche multiplied by the high electric field $E_{\rm GEM}$ in the holes of the THGEM film. The multiplied electrons are extracted and drift towards the anode due to the electric field $E_{\rm ind}$. The multiplication gain can reach up to 10^4 with a single thinner-THGEM layer.

The stability of such a detector over 14 h was measured *via* a collimated ^{55}Fe X-ray source with a rate of 400 photons mm^{-2} s^{-1}. The thinner-THGEM operated with a stable gain with a fluctuation lower than 10% (Liu *et al.*, 2012).

Two main factors can influence the intrinsic resolution of the THGEM: (i) the nature of the gas mixture affects the transverse electron diffusion (Silva *et al.*, 2013; Carramate *et al.*, 2017); (ii) the geometry is decided by the hole diameter and the pitch is related to the charge spread and sharing (Lopes *et al.*, 2013; Moleri *et al.*, 2017). The intrinsic resolution generally ranges from one hundred to several hundred micrometres.

Two thinner-THGEM elements can be used in cascade. This double-THGEM structure offers higher detector gains with each THGEM element operating at a lower voltage bias (Breskin *et al.*, 2009). This leads to higher operation stability in large dynamic applications, especially in single-photon measurements (Chechik *et al.*, 2005) and neutron imaging (Israelashvili *et al.*, 2017).

The detector is designed to have a sensitive area of 16.0 cm × 1.6 cm and is curved with a radius of 20 cm, corresponding to an open angle of 19.2°. The total number of anode strips is 320 and each strip corresponds to an open angle of 0.15°. Two curved acrylic frames are placed between them to guarantee

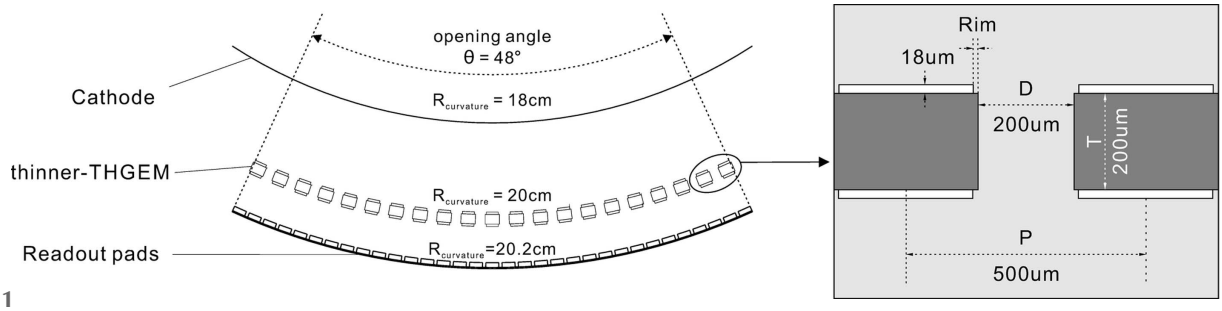

Figure 1
Scheme of a thinner-THGEM.

the parallelism of each layer. The detector is sealed in an acrylic box of size 19.7 cm × 9.5 cm × 5 cm; X-rays are introduced through a 50 µm Mylar film window. A CAEN N1471 power supply was used to apply a high voltage to the cathode and thinner-THGEM films. A gas mixture of Ne/CH_4 (95:5) was flushed into the detector and the gas flow was set to 10 ml min^{-1}.

3. Experimental setup

A scheme and photographs of the setup are shown in Figs. 2 and 3, respectively. The powdered crystal sample is placed perpendicular to the incident beam. The thinner-THGEM detector is fixed on a platform which can rotate around the sample with a distance of 20 cm between the cathode of the detector and the sample.

For synchrotron radiation applications, the detector receives the X-ray photons within a fixed time interval because of the the regular time structure of BSRF. The flux is expected to be 1×10^{11} at 8 keV. The signals collected at the anode are sent to a pico-ampere precise DC readout FEE board based on DDC232 chips. Each FEE board has 32 current input channels. The current signal is integrated every 166 µs and is converted into a integrated charge value. An FPGA-Altera module accepts the FEE readout. The data acquisition (DAQ) rate is 1 kHz.

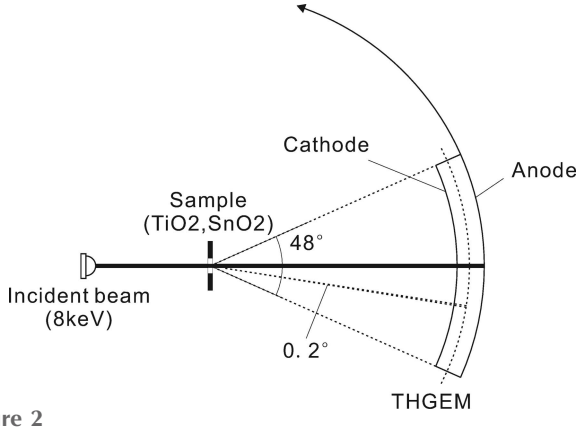

Figure 2
Scheme of the THGEM test arrangement.

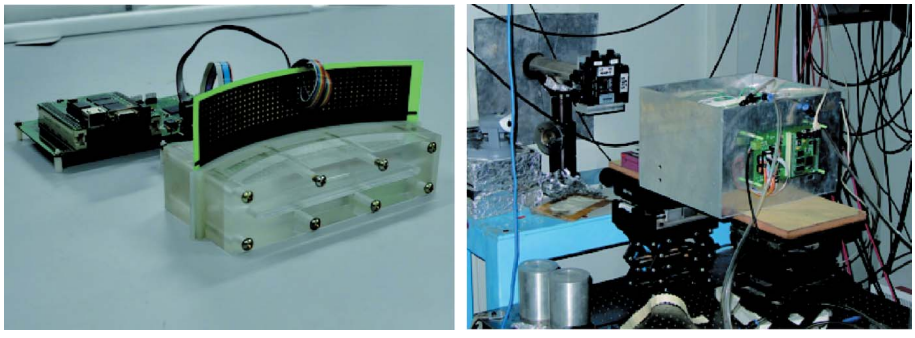

Figure 3
Photographs of the diffraction meter. (Left) The combined thin-THGEM construction and (right) the device mounted on the synchrotron radiation beam.

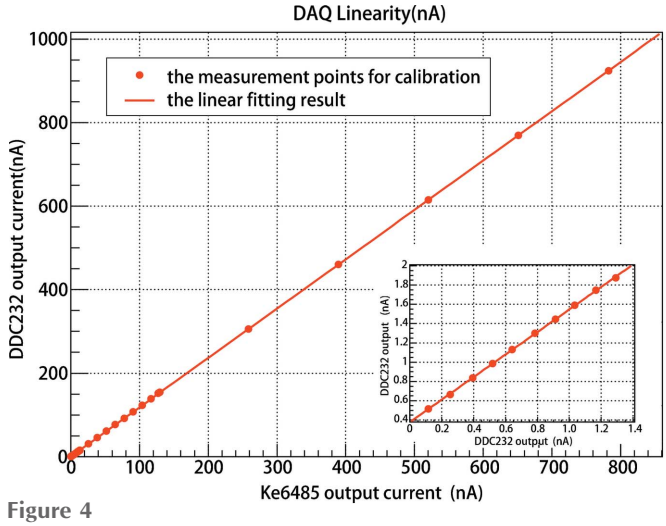

Figure 4
Calibration of the DAQ system.

The DAQ system is calibrated using a KE6485 pico-ammeter with 10 fA resolution. The results are given in Fig. 4, showing that the sensitivity of the current per channel ranges from 100 pA to 800 nA with good linearity.

4. Measurements of spatial resolution

Titanium dioxide (TiO_2) powder was used to measure the spatial resolution of the detector as a function of scattering angle. For this study the detector was firstly operated in ionization mode by setting $V_{THGEM} = 0$ for measuring the incident synchrotron radiation beam light directly. The beam spread (Fig. 5) was fitted to be $0.968 \pm 0.002^\circ$ full width at half-maximum (FWHM) by a simple Gaussian (Liu *et al.*, 2013). The detector was then operated in avalanche mode by increasing V_{THGEM} to 400 V and rotating the detector to about $\pm 25^\circ$, which is the strongest diffraction peak of TiO_2 powder. The peak was fitted with a single Gaussian convolved with the beam spread.

The fitting centroid is 25.376° and the spatial resolution has a FWHM of $0.348 \pm 0.191^\circ$ (Fig. 6), which is consistent with the powder diffraction file (PDF) data (Wyckoff, 1963) within one standard deviation. The spatial resolution of 0.148° is much less than the uncertainty derived from parallax, *i.e.* 0.78°, proving that the system errors from the parallax are reasonably well suppressed.

5. Measurements of powder diffraction spectra

In order to detect the weak diffraction peaks, a higher gain and better noise–signal ratio are necessary. Therefore a cascade structure, called a double-THGEM, is applied.

The setup is shown in Fig. 7. The detector gain was obtained *via* current measurement. In contrast with the

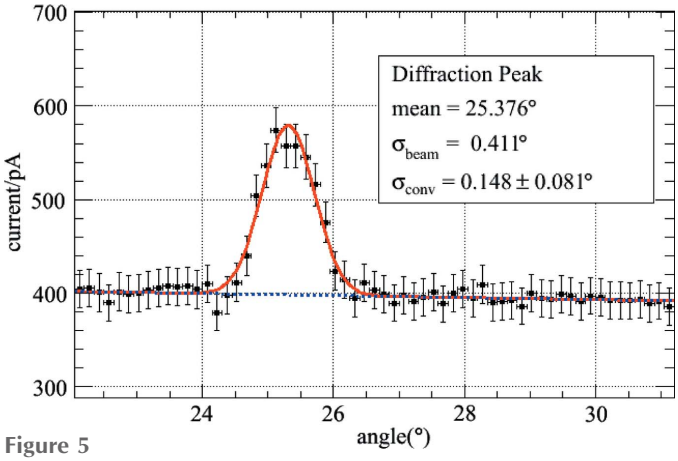

Figure 5
Direct beam and the TiO_2 peak.

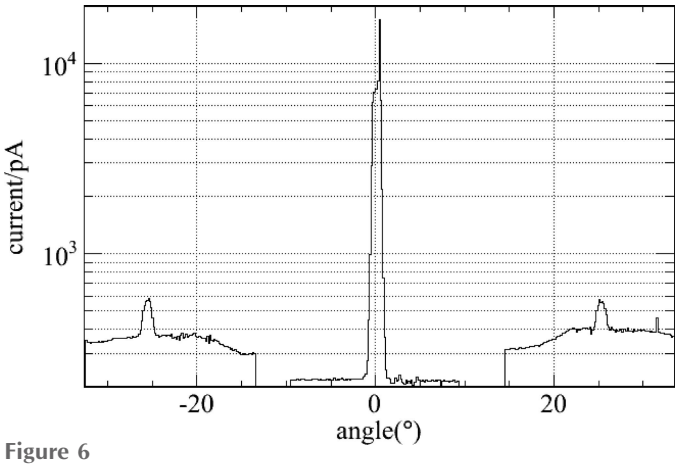

Figure 6
Fitting result of the spatial resolution.

completed preliminary work, the sensitivity of the double-THGEM instrument can reach eight times higher than that of the former single-THGEM board mode. To eliminate the diffuse scattering background, spectra with and without the sample are measured. The real diffraction spectrum is the difference between these two. To scan the whole range of 48°, the chamber should be rotated along the arc.

Figs. 8 and 9 show calculation of the diffraction angle from the PDF and the spectra for TiO_2 and SnO_2 detected by the THGEM-based X-ray diffraction meter. The peak positions and widths are listed in Tables 1 and 2. As shown in Figs. 10 and 11, the results are consistent with the calculation from

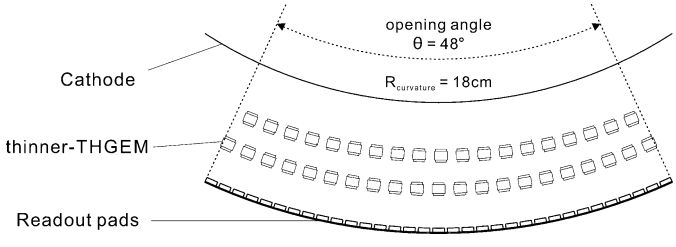

Figure 7
Scheme of the double-THGEM detector.

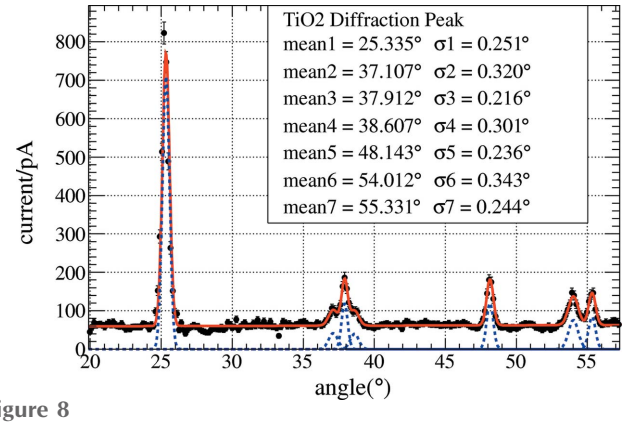

Figure 8
Powder diffraction spectra of TiO_2.

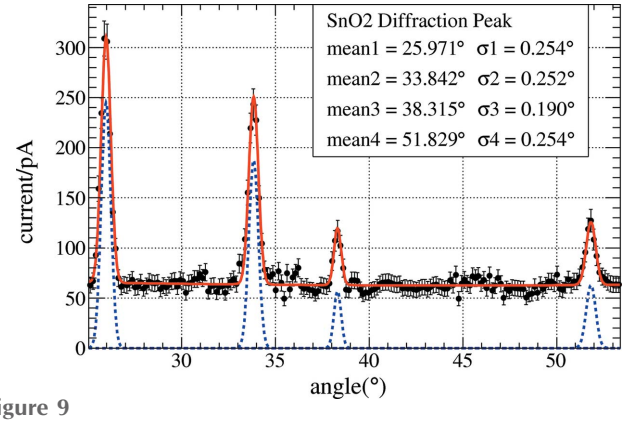

Figure 9
Powder diffraction spectra of SnO_2.

PDF99-0008 (Wyckoff, 1963) and PDF99-0024 (Baur & Khan, 1971).

Fig. 12 shows a comparison of the resolution and the calculated error of a flat-plate detector. The system errors from the parallax are obviously suppressed.

6. Asymmetric-effect correction

The width of the detector implies asymmetric peaks since the radius of the diffraction rings is not very large compared with the width of the readout strip. This effect is corrected using the following method.

The Monte Carlo method was adopted to simulate this distortion. Events are generated randomly according to the beam-spread shape, shooting at a particular diffraction angle, projecting to the detector and recording the hit positions. A digitization algorithm is then performed to simulate the detector response. Two million events were generated to minimize the statistical error. For example, the simulation result of the diffraction peak at 25.3° is shown in Fig. 13 with a visible asymmetric distribution.

The measured intensity distribution is then fitted by

$$I(x) = n_{\rm sig}\, F(x;\theta) \otimes G(x;0,\sigma) + n_{\rm bg} C(x).$$

Here, $F(x;\theta)$ is the distribution simulated from the Monte Carlo method, $G(x;0,\sigma)$ is the detector resolution, $C(x)$ is a

Table 1
Diffraction spectrum for sample TiO_2 with Cu $K\alpha_1$ radiation.

2Θ	Intensity	FHWM
25.335°	100	0.591°
37.107°	7.44	0.754°
37.912°	14.31	0.509°
38.607°	6.67	0.709°
48.143°	15.80	0.556°
54.012°	14.47	0.808°
55.331°	11.44	0.575°

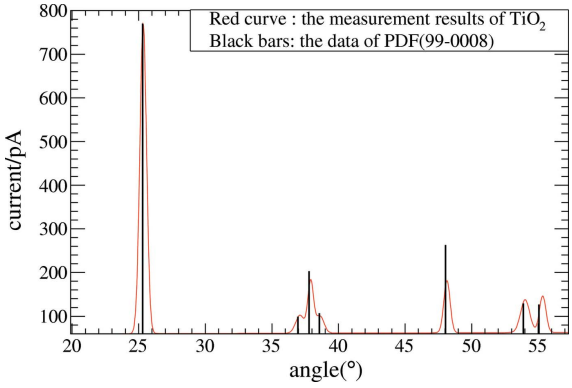

Figure 10
Comparison between the TiO_2 spectrum and the powder diffraction file.

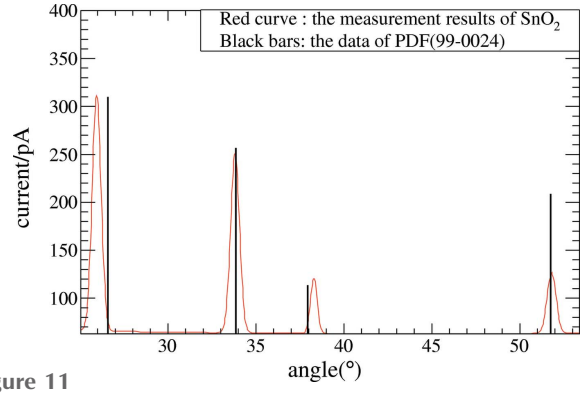

Figure 11
Comparison between the SnO_2 spectrum and the powder diffraction file.

Chebyshev polynomial (the background shape), and n_{sig} and n_{bg} are the number of events for the signal and the background, respectively. The two main peaks for TiO_2 at 25.3° and 48.1° are corrected using this method. The differences between the angular resolution with and without correction $(\sigma_w^2 - \sigma_{wo}^2)^{1/2}$ *versus* the diffraction angle are shown in Table 3.

7. Conclusions and prospects

The results of two typical samples TiO_2 and SnO_2 demonstrate that the DC-mode THGEM detector working at a frame rate of 1 kHz was sensitive enough to observe the main powder diffraction peaks, and the angular resolution can reach $0.148 \pm 0.081°$ for large open-angle ranges without parallax errors. Moreover, the large dynamic range enables the strong direct synchrotron radiation beam and the weak diffraction peaks to be measured with the same detector and same device layout simultaneously without any collimator.

Some of our experiments and facilities are under research or to be published specifically for X-ray application, such as grazing-incidence X-ray diffraction measurements with high spatial resolution, small-angle X-ray scattering with a large dynamic range, sealed xenon-gas THGEM detectors for X-ray

Table 2
Diffraction spectrum for sample SnO_2 with Cu $K\alpha_1$ radiation.

2Θ	Intensity	FHWM
25.971°	100	0.598°
33.842°	75.93	0.593°
38.315°	17.40	0.447°
51.829°	25.55	0.598°

Table 3
Correction diffraction spectrum for sample TiO_2 with Cu $K\alpha_1$ radiation.

2Θ	Intensity	FHWM
25.271°	100	0.598°
37.094°	7.44	0.520°
37.912°	14.31	0.586°
38.630°	6.67	0.770°
48.136°	15.80	0.562°
54.000°	14.47	0.794°
55.298°	11.44	0.569°

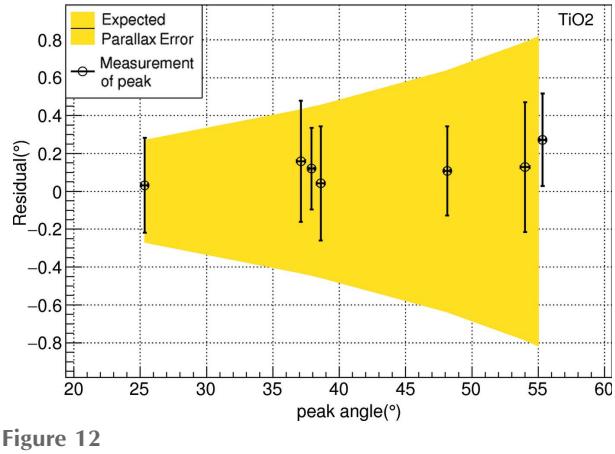

Figure 12
The shape of the asymmetric diffraction peak.

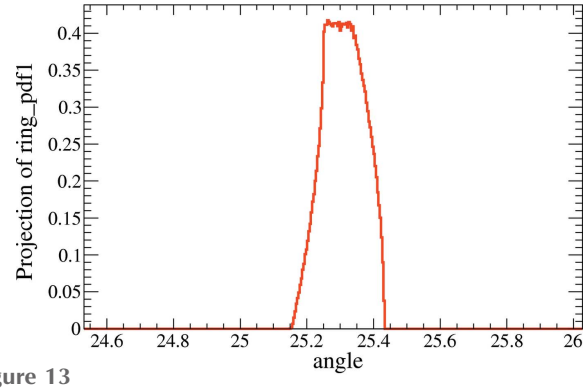

Figure 13
Suppression of parallax error.

(>20 keV) measurements, and a compact facility with a one-dimensional 512 channel digital readout diffraction meter for detecting outdoor weak X-ray mineral samples. In other fields, some two-dimensional larger-area image detectors for high-energy physics, radiation hazard distribution monitors and neutron detection are under research. The prospect is broad and bright.

Acknowledgements

We are grateful to all colleagues at the laboratory 1W2B of the Beijing Synchrotron Radiation Facility. We would like to express sincere appreciation to A. Breskin of the Weizmann Institute for stimulating discussions and encouragement; P. Picchi and Rui de Oliveira of CERN for their kind support; and S. Dalla Torre and S. Levorato of Trieste for helpful discussions.

Funding information

This work was supported by the National Natural Science Foundation of China (Grant Nos. 11575193, 11205240), the Youth Innovation Promotion Association of CAS (No. 2016153) and the Natural Science Key Foundation of Guangxi (Grant No. 2015GXNSFDA139002).

References

Alexeev, M., Alfonsi, M., Birsa, R., Bradamante, F., Bressan, A., Chiosso, M., Ciliberti, P., Croci, G., Colantoni, M. L., Torre, S. D., Denisov, O., Pinto, S. D., Duic, V., Ferrero, A., Finger, M., Finger, M. Jr, Fischer, H., Giacomini, G., Giorgi, M., Gobbo, B., Hagemann, R., Heinsius, F. H., Herrmann, F., Jahodova, V., Königsmann, K., Kramer, D., Lauser, L., Levorato, S., Maggiora, A., Martin, A., Menon, G., Mutter, A., Nerling, F., Panzieri, D., Pesaro, G., Polak, J., Rocco, E., Ropeleswki, L., Sauli, F., Sbrizzai, G., Schiavon, P., Schill, C., Schopferer, S., Slunecka, M., Sozzi, F., Steiger, L., Sulc, M., Takekawa, S., Tessarotto, F. & Wollny, H. (2010). *J. Instrum.* **5**, P03009.

Baur, W. H. & Khan, A. A. (1971). *Acta Cryst.* B**27**, 2133–2139.

Breskin, A., Alon, R., Cortesi, M., Chechik, R., Miyamoto, J., Dangendorf, V., Maia, J. & Dos Santos, J. M. F. (2009). *Nucl. Instrum. Methods Phys. Res. A*, **598**, 107–111.

Carramate, L., Silva, A., Azevedo, C., Fortes, I., Monteiro, S., Sousa, S., Ribeiro, F., Francesco, S. D., Covita, D. & Veloso, J. (2017). *J. Instrum.* **12**, T05003.

Cernik, R. J., Murray, P. K., Pattison, P. & Fitch, A. N. (1990). *J. Appl. Cryst.* **23**, 292–296.

Chechik, R., Breskin, A. & Shalem, C. (2005). *Nucl. Instrum. Methods Phys. Res. A*, **553**, 35–40.

Chechik, R., Breskin, A., Shalem, C. & Mormann, D. (2004). *Nucl. Instrum. Methods Phys. Res. A*, **535**, 303–308.

Collins, S. P., Cernik, R. J., Pattison, P., Bell, A. M. T. & Fitch, A. N. (1992). *Rev. Sci. Instrum.* **63**, 1013–1014.

Duarte Pinto, S., Villa, M., Alfonsi, M., Brock, I., Croci, G., David, E., de Oliveira, R., Ropelewski, L., van Stenis, M. & Taureg, H. (2009). *J. Instrum.* **4**, P12006.

Israelashvili, I., Coimbra, A. E. C., Vartsky, D., Arazi, L., Shchemelinin, S., Caspi, E. N. & Breskin, A. (2017). *J. Instrum.* **12**, P09029.

Liu, H. B., Liu, Q., Chen, S., Ruan, X. D., Nicholson, C., Xie, Y. G., Zheng, Y. H., Zheng, Z. P., Lu, J. G., Zhou, L., Tang, A. S., Yang, Y. D., Dong, Y. & Li, M. (2012). *J. Instrum.* **7**, C06001.

Liu, H. B., Zheng, Y. H., Xie, Y. G., Zheng, Z. P., Lu, J. G., Zhou, L., Yu, B. X., Tang, A. S., Yang, Y. D., Dong, Y. & Li, M. (2011). *Nucl. Instrum. Methods Phys. Res. A*, **659**, 237–241.

Liu, Q., Liu, H. B., Chen, S., Xie, Y. G., Zheng, Y. H., Zhou, X. K., Wang, B. L., Huang, W. Q., Zhang, Y. D., Ge, D. S., Zhou, X., Zhang, Z. Y., Dong, Y., Zhang, Q., Chang, J., Li, M. & Wang, J. (2013). *J. Instrum.* **8**, C11008.

Lopes, T., Silva, A. L. M., Azevedo, C. D. R., Carramate, L. F. N. D., Covita, D. S. & Veloso, J. F. C. A. (2013). *J. Instrum.* **8**, P09002.

Moleri, L., Bhattacharya, P., Coimbra, A., Breskin, A. & Bressler, S. (2017). *J. Instrum.* **12**, P10017.

Roessle, M. W., Klaering, R., Ristau, U., Robrahn, B., Jahn, D., Gehrmann, T., Konarev, P., Round, A., Fiedler, S., Hermes, C. & Svergun, D. (2007). *J. Appl. Cryst.* **40**, s190–s194.

Silva, A. L. M., Azevedo, C. D. R., Carramate, L. F. N. D., Lopes, T., Castro, I. F., de Oliveira, R. & Veloso, J. F. C. A. (2013). *J. Instrum.* **8**, P05016.

Wyckoff, R. W. G. (1963). *Crystal Structures*, Vol. 1, pp. 253–254. New York: Interscience.

Zhang, A. W., Yu, B. X., Xie, Y. G., Liu, H. B., An, Z. H., Wang, Z. G., Cai, X., Sun, X. L., Shi, F., Fang, J., Xue, Z., Lü, Q., Sun, L., Ge, Y., Liu, Y., Hu, T., Zhou, L. & Lü, J. (2012). *Chin. Phys. C.* **36**, 142–145.